G. Di Martino and A. Iodice, “Coprime Synthetic Aperture Radar (CopSAR): A New Acquisition Mode for Maritime Surveillance”, *IEEE Trans. Geosci. Remote Sens.*, vol. 53, no. 6, pp. 3110-3123, June 2015.
DOI: 10.1109/TGRS.2014.2369035.

Coprime Synthetic Aperture Radar (CopSAR): a New Acquisition Mode for Maritime Surveillance

Gerardo Di Martino, *Member, IEEE*, Antonio Iodice, *Senior Member, IEEE*

Abstract — **In this paper we propose a Synthetic Aperture Radar (SAR) technique able, in the case of bright targets over a dark background, to reduce the amount of data to be stored and processed, and, at the same time, to increase the range swath, with no geometric resolution loss. Accordingly, the proposed approach can be usefully employed in ocean monitoring for ship detection. The technique consists of a new SAR acquisition mode and of a very simple processing. It is based on the adaptation of the coprime array beamforming concept to the case of SAR systems: two interlaced sequences of pulses are transmitted, with two sub-Nyquist PRFs that are equal to the Nyquist PRF divided by two coprime integer numbers. Each sequence is separately processed via standard SAR processing, and the two final aliased images are combined in a very simple way to cancel aliasing. We call the proposed approach "Coprime SAR" (CopSAR). Three different implementations are proposed, and the effectiveness of the CopSAR concept is demonstrated by using both simulated and real SAR data. It turns out that the significant data amount reduction and range swath increase are only paid with a reduction of the target-to-background ratio and with the presence of a (non stringent) limit on ship azimuth size.**

***Index Terms*— Synthetic Aperture Radar (SAR), coprime sampling, maritime applications.**

I. INTRODUCTION

OCEAN surface monitoring for ship detection via Synthetic Aperture Radar (SAR) [1]-[3] is gaining an increasing interest in the remote sensing scientific community, due to its importance in maritime traffic control, border surveillance, fisheries control, and search and rescue. This application calls for both wide coverage and high resolution, which imply a huge amount of data to be stored and processed. Therefore, the development of techniques able to reduce the amount of data is highly desired. In addition, methods to extend the size of the range swath, and more in general the coverage, of SAR systems are certainly welcomed. Accordingly, in recent years different techniques have been proposed with the aim of increasing coverage: array beamforming [4]-[5], staggered SAR [6], MIMO SAR [7]-[8], SAR constellations [9]; however, these methods have the drawbacks of further increasing the data amount, and of significantly complicating hardware and/or processing. On the other

The authors are with the Dipartimento di Ingegneria Elettrica e delle Tecnologie dell'Informazione, Università di Napoli Federico II, 80125, Napoli, Italy (e-mail: gerardo.dimartino@unina.it; iodice@unina.it).

hand, some techniques to reduce data amount have been also proposed: on-board presumming and/or prefiltering techniques [10]-[11] are certainly useful to this aim, but they imply a resolution loss; more recently, compressive sensing has been also proposed to focus sparse targets [12]-[14]: this allows in principle for a reduction of data amount, but it significantly complicates processing.

Actually, it is well-known that a simple way to both reduce data amount and, at the same time, extend the range swath by reducing range ambiguity does exist: it just consists in reducing the Pulse Repetition Frequency (PRF). However, it is also well-known that, unfortunately, reducing the PRF under the Nyquist rate, i.e., under the SAR system Doppler bandwidth, causes the aliasing phenomenon, that in this case is usually referred to as azimuth ambiguity [15]. Therefore, a reduction of the PRF is usually not a viable solution, although using a sub-Nyquist PRF at the cost of allowing for azimuth ambiguities has been recently proposed for ship detection applications [16].

In this paper we propose a technique able, in the case of bright targets over a dark (not necessarily homogeneous) background, which is the case for the ship detection application, to reduce the amount of data and, at the same time, to increase the range swath, with no geometric resolution loss: this is obtained by reducing both range ambiguity, caused by the partial superposition, at the receiver, of echoes of consecutively transmitted pulses, and azimuth ambiguity, caused by sub-Nyquist PRF. The proposed technique is based on the adaptation of the coprime array beamforming concept [17]-[18] to the case of SAR systems: two interlaced sequences of pulses are transmitted, with two sub-Nyquist PRFs that are equal to the Nyquist PRF divided by two coprime integer numbers. Each sequence is separately processed via standard SAR processing, and the two final aliased images are combined in a very simple way to cancel aliasing, as explained in the following sections. The proposed solution has the additional advantage of requiring no, or a minimum, increase of software/hardware complexity: in its simplest implementation, see Section III, it can be even applied to currently available sensors (although in this case only to reduce the data amount, with no increase of range swath). We will show that the significant data amount reduction and range swath increase are only paid with a reduction of the target-to-background ratio and with the presence of a (non stringent) limit on ship azimuth size.

At the best of the authors' knowledge, this is the first time that such a solution is proposed. We call the proposed approach “Coprime SAR” (CopSAR).

The paper is organized as follows. In Section II the basic rationale of the proposed method is illustrated. In Section III, three possible implementations of the CopSAR concept are proposed and discussed, and in Section IV meaningful experiments on both simulated and real data are presented. Finally, conclusions are reported in Section V.

II. CopSAR rationale

It is well-known that replicas of the reflectivity pattern appear on SAR images due to the finite PRF. Such replicas are shifted

both in azimuth, and, although in a smaller extent, in range [15]. In particular, the azimuth and range shifts of the *i*th replica are [15], [19]

$$\Delta x_i = i\frac{\mathrm{PRF}\lambda r_0}{2v} \tag{1}$$

and

$$\Delta r_i = \frac{\Delta x_i^2}{2r_0}\ , \tag{2}$$

where λ is the electromagnetic wavelength, r_0 is the closest range between the platform and the center of the real antenna footprint, and v is the uniform sensor velocity. However, these replicas are slightly defocused for $i \neq 0$, and they are weighted by the real antenna azimuth pattern (AAP): therefore, an ideal AAP that is null outside its main beam (i.e., that has no sidelobes) suppresses all replicas of order i such that $|\Delta x_i| > X$, where $X=\lambda r_0/L$ is the real antenna footprint azimuth size, L being the azimuth real antenna length, and only replicas of order i such that $|i| \leq M$ are present, where M is the largest integer such that $|\Delta x_M| < X$. In practice, the ideal AAP condition can be only approached (by using an antenna with a high peak-to-sidelobe ratio), but it can never be exactly achieved. However, replicas of order higher than M are strongly attenuated, and for the moment being we will neglect them.

In view of the considerations above, SAR systems are usually designed to satisfy the condition

$$\frac{\mathrm{PRF}\lambda r_0}{2v} \geq X\ , \quad \text{i.e.,} \quad \mathrm{PRF} \geq \frac{2v}{L}, \tag{3}$$

so that $M = 0$ and no replica, i.e., no aliasing, is present (indeed, $2v/L$ is the SAR signal Doppler bandwidth, i.e., its Nyquist rate).

In conclusion, assuming an ideal AAP, if condition (3) is not satisfied, then $2M$ target replicas appear, that are spatially displaced in azimuth according to (1) and, in a lesser extent, in range according to (2). If, as it is usually the case, condition (3) is satisfied, then M=0 and no replica is present: only the actual, correctly focused, targets appear in the image.

Here, we propose a SAR acquisition modality in which the system transmits two interlaced sequences of pulses: one at $\mathrm{PRF}_1=\mathrm{PRF}_0/N_1$, and the other at $\mathrm{PRF}_2=\mathrm{PRF}_0/N_2$, where PRF_0 satisfies the Nyquist condition (3), i.e., $\mathrm{PRF}_0 \geq 2v/L$, and N_1 and N_2 are two coprime integers (i.e., their greatest common divisor is 1). This is realized by transmitting pulses at times $t_n=n/\mathrm{PRF}_0$ only if n is an integer multiple of N_1 or N_2 (i.e., $n=n_1 N_1$ or $n=n_2 N_2$, with n_1 and n_2 integer), instead that for all integer values of n, as it is the case for the standard acquisition mode, see Fig.1. The two sequences can be separately processed to obtain two SAR

images, $s_1(x,r)$ and $s_2(x,r)$. Here, x and r are the azimuth and range coordinates, respectively. Geometric resolution of these images will not be changed with respect to the standard SAR case, because the synthetic array length is unchanged[1], but of course these images will be severely aliased. However, if the scene consists of bright targets on a dark background (as in the case of boats or ships on the ocean), then only the true targets will be present on both aliased images at the same location, whereas aliased targets (i.e., replicas) will be at different locations on the two images. In fact, on the first image, i.e., $s_1(x,r)$, each target gives rise to replicas displaced as (see also Fig.3)

$$\Delta x_{i_1} = i_1 \frac{\mathrm{PRF}_0 \lambda r_0}{N_1 2v} \quad , \quad \Delta r_{i_1} = \frac{\Delta x_{i_1}^2}{2r_0} \quad , \tag{4}$$

whereas on the second image, i.e., $s_2(x,r)$, each target gives rise to replicas displaced as

$$\Delta x_{i_2} = i_2 \frac{\mathrm{PRF}_0 \lambda r_0}{N_2 2v} \quad , \quad \Delta r_{i_2} = \frac{\Delta x_{i_2}^2}{2r_0} \quad , \tag{5}$$

with i_1 and i_2 integers, so that replicas on the two images will not be at the same location unless $i_1/\, i_2 = N_1/\, N_2$. But, since N_1 and N_2 are coprime, this only happens if $i_1 = i\, N_1$ and $i_2 = i\, N_2$, so that

$$\Delta x_{i1} = \Delta x_{i2} = i \frac{\mathrm{PRF}_0 \lambda r_0}{2v} \quad , \tag{6}$$

i.e., only at the positions of the replicas in the image that would be obtained in the standard acquisition mode, see (1). And, since $\mathrm{PRF}_0 \geq 2v/L$, these replicas are suppressed (in practice, strongly attenuated) by the AAP. Therefore, if we combine the two aliased images by choosing, at each pixel, the image value from the image in which its modulus is smaller, i.e.,

$$s(x,r) = \begin{cases} s_1(x,r) & \text{if} \quad |s_1(x,r)| < |s_2(x,r)| \\ s_2(x,r) & \text{otherwise} \end{cases} \quad , \tag{7}$$

then we obtain a final image $s(x,r)$ in which no replicas are present. As a matter of fact, where in one of the two images there is a target replica, in the other one there is only the sea background, and selecting the smallest modulus we correctly select the sea background. Conversely, where the true target is present, both images have similar, high moduli, and even selecting the smallest

[1] Note that, although the two sequences are sub-sampled, the entire SAR system bandwidth must be processed to maintain the original resolution. The simplest way to do this (although not the most efficient one) is to add zeroes in the place of missing pulses and process the data exactly as in the standard SAR case.

one we correctly obtain a brilliant pixel.

It must be noted that an even more favorable situation, in which replicas in the two images obtained from the subsampled raw signals are never at the same location, would be obtained by using two sub-Nyquist PRFs whose ratio is an irrational number. However, using the proposed CopSAR modality instead of the irrational PRFs ratio approach is convenient for two reasons. First of all, implementation of CopSAR, and the switching between CopSAR and standard SAR, are much simpler, since a single clock at rate PRF_0, combined with a very simple control logic (necessary to implement the simple rule for the selection of pulse transmission times described above), can be employed. In addition, some important properties regarding data amount reduction, minimum time separation between pulses and minimum space separation between replicas can be easily derived in the CopSAR case (at variance with the irrational PRFs ratio approach), and they can be used to guide the implementation of the method, see Section III, and to evaluate its expected performance and validity limits, as discussed in the following.

With regard to data amount reduction, it is easy to realize that the ratio R between the number of pulses transmitted in the CopSAR mode and in the standard SAR acquisition mode is

$$R = \frac{1}{PRF_0}\left(\frac{PRF_0}{N_1} + \frac{PRF_0}{N_2} - \frac{PRF_0}{N_1 N_2}\right) = \frac{N_1+N_2-1}{N_1 N_2} \quad , \tag{8}$$

where the last subtracting term is due to the fact that the two sub-sequences of pulses share one pulse every N_1N_2, see Fig.1.

Let us now consider the time separation between pulses. In view of the rule for the selection of pulse transmission times described above, it is given by

$$t_{n_1} - t_{n_2} = \frac{n_1 N_1 - n_2 N_2}{\mathrm{PRF}_0} \quad . \tag{9}$$

The difference at the numerator of (9) assumes the values 0, ±1, ±2, etc., (with the exception of very few "holes", see [17]-[18]) once every N_1N_2/PRF_0 seconds. Accordingly, the minimum time separation between consecutive pulses is $1/\mathrm{PRF}_0$, and this happens twice every N_1N_2 pulses (once when the numerator of (9) is +1 and once when it is –1, see also Fig.1).

Finally, the distance Δ between replicas can be easily obtained by using (4) and (5) as follows

$$\Delta = \Delta x_{i_1} - \Delta x_{i_2} = i_1 \frac{\mathrm{PRF}_0 \lambda r_0}{N_1 2v} - i_2 \frac{\mathrm{PRF}_0 \lambda r_0}{N_2 2v} = \frac{\mathrm{PRF}_0 \lambda r_0}{2v}\left(\frac{i_1 N_2 - i_2 N_1}{N_1 N_2}\right) \quad , \tag{10}$$

and the minimum distance between consecutive replicas (see also Fig.3) is achieved when the absolute value of the numerator in

the parenthesis of (10) is equal to unity, so that it is

$$\Delta_{min} = \frac{\mathrm{PRF}_0 \lambda r_0}{N_1 N_2 2v} \quad . \tag{11}$$

This value sets the maximum allowed azimuth size of the bright target to avoid partial overlapping of replicas in the two images obtained from the subsampled raw signals. Note that, since PRF_0 satisfies condition (3), Δ_{min} is greater than the azimuth footprint divided by N_1N_2. The value in (11) sets a trade-off between data amount reduction, for which high values of N_1 and N_2 are desirable, and maximum azimuth size of targets, which increases if N_1 and N_2 are decreased. Another factor that limits the values of N_1 and N_2 is the target-to-background ratio (TBR) over the two images obtained from the subsampled raw signals: in fact, if the number of samples used to focus the image is reduced by a factor N_1 or N_2, then also the TBR is reduced by the same factor (see [2] and Appendix A). This also leads to use very close values of N_1 and N_2 (maybe differing by one), so to obtain very similar TBRs on the two aliased images. In the following, with no loss of generality, we will assume that $N_1 < N_2$, so that our suggestion is to set $N_2 = N_1 + 1$. With this regard, it is interesting to analytically evaluate the TBR and analyze the background statistics in the final CopSAR image, obtained by using the rule of (7). This analysis is carried out in detail in Appendix A. It turns out that in the final CopSAR image the TBR is reduced by a factor of the order of $N_2^2/(N_1 + N_2)$ with respect to the standard SAR image. For $N_2 = N_1 + 1$, this corresponds to about $N_2/2$. In addition, it turns out that in the CopSAR image background the speckle tends to be fully developed even when it is not in the standard SAR image.

At this point it is important to underline that the proposed method does not require that the sea background is a homogeneous dark distributed target, but just that it is a distributed target darker than the ship (which, for ship detection, is required even in the standard SAR case). It must be also noted that sub-sampling and consequent aliasing have the effect of blurring large complex distributed targets: in fact, replicas of different parts of the distributed target overlap one on another, contrarily to what happens for smaller targets, like the ships, provided that they are smaller than the value given by (11). Therefore, the sea background appears more homogeneous in CopSAR than in standard SAR images, and an example of this effect will be presented in Section IV. In conclusion, the presence of a complex sea signature (which is not uncommon, due to internal waves, low wind areas, strong wave patterns and other phenomena) is not really an issue for our method; in addition, although the average TBR is decreased in the CopSAR case, locally this may possibly not be the case, due to the blurring of the sea signatures.

It is also worth noting that, if different bright targets of finite sizes are present in the scene, the very unfortunate circumstance may happen that a replica of one target in the first image, $s_1(x,r)$, overlaps with a replica of another target in the second image, $s_2(x,r)$: this causes the appearance, on the combined image $s(x,r)$, of a "ghost", i.e., of a false bright target. However, these "ghosts" can be distinguished from true bright targets by computing the correlation coefficient between $s_1(x,r)$ and $s_2(x,r)$ over a

window in correspondence of each bright spot of $s(x,r)$: if the bright spot is a true target, the correlation coefficient will be practically unitary (because exactly the same pattern will be present on the two complex images), otherwise it will be significantly smaller than one (because two different patterns will be present on the two complex images). A similar discussion holds for the very unfortunate case of a vessel of size and orientation such that condition (11) is not satisfied: the true target will perfectly overlap on the two images, so that a unitary correlation coefficient is expected, whereas replicas will not perfectly overlap, so that ghosts will have a smaller correlation coefficient. This will be illustrated by an example in Section IV.

Finally, a discussion on the effects of possible vessel motion is in order. In fact, an unknown across-track velocity component of the ship will create a dislocation from the true position, and an unknown along-track velocity component will defocus the ship. However, displacement due to an unknown across-track velocity component will be with very good approximation the same for both the real target and the replicas, so that distances between replicas are not changed and the CopSAR method still works. Target defocusing due to an unknown along-track velocity component will cause an increase of the apparent target size and a reduction of its apparent radar cross section (RCS). However, replicas of dynamic targets, even if defocused due to their movement, will not overlap if their overall (i.e., including defocusing) azimuth size is smaller than the value given by (11), so this is not a critical issue for small dynamic vessels, but it might be for very large dynamic ships aligned along the azimuth direction. Conversely, reduced RCS may actually be a problem for small dynamic targets in view of the reduced target-to-sea ratio in CopSAR images, but it is not a critical issue for very large, brilliant, dynamic targets.

III. Proposed Implementations

The simplest implementation of the CopSAR concept, which we define “basic implementation”, is to directly apply the procedure defined in the previous section and illustrated in Fig.1: this allows a reduction of the amount of data to be stored and processed equal to the ratio R given in (8). This can be implemented on-board by transmitting only the necessary pulses, or in the ground segment, by decimating the original received pulses sequence. The former solution is certainly more attractive, since it allows a reduction of required on-board memory, of required power, and of required data downlink capacity: for a mission still to be launched, this would be the obvious choice. However, decimation of the full sequence at the ground segment allows for the reduction of data mass storage on ground (which is not a bottle-neck, but whose reduction is certainly useful to avoid overload of large raw data archives) even for currently existing sensors. We will show an example of that in the next section.

This “basic” implementation only reduces the amount of data to be stored and processed, but it does not allow for an extension of the range swath, because the minimum time separation between consecutive pulses is $1/\mathrm{PRF}_0$, as in the case of standard SAR. However, at variance with the standard SAR case, this minimum separation only happens twice every N_1N_2 pulses. Accordingly,

in order to double the range swath, we propose a second implementation, in which, in the sequence of pulses transmitted at rate PRF_0/N_1, those pulses that would be separated by just $1/\mathrm{PRF}_0$ from a pulse of the other sequence are not transmitted. Therefore, in the first sequence 2 pulses every N_1N_2 will be missing, see Fig.2. This sequence can be seen as the difference (i.e., subtraction) between a sequence at rate PRF_0/N_1 and two interlaced sequences at rate $\mathrm{PRF}_0/(N_1N_2)$. Accordingly, in the image $s_1(x,r)$ each bright target will have not only replicas displaced according to (5), but also replicas at distances

$$\Delta x_{i_{12}} = i_{12}\frac{\mathrm{PRF}_0\lambda r_0}{N_1N_2 2v} \quad , \quad \Delta r_{i_{12}} = \frac{\Delta x_{i_{12}}^2}{2r_0} \quad , \tag{12}$$

and these replicas will overlap with a replica of the second image for $i_{12}= i_2\, N_1$, so that on the final image $s(x,r)$ each true bright target will have a maximum of $2(N_2-1)$ "ghosts". However, these ghosts will be attenuated with respect to the true target by a factor N_2 due to the reduced number of pulses that contribute to focus them (in addition to attenuation due to the slight replica defocusing). In addition, the data reduction rate of (8) is further decreased as

$$R = \frac{1}{PRF_0}\left(\frac{PRF_0}{N_1} + \frac{PRF_0}{N_2} - 3\frac{PRF_0}{N_1N_2}\right) = \frac{N_1+N_2-3}{N_1N_2} \quad , \tag{13}$$

In conclusion, in this second implementation the minimum time separation between consecutive pulses is $2/\mathrm{PRF}_0$, so that the range swath can be doubled, and data reduction rate is further slightly reduced, but this is paid with the appearance of ghosts, that however are significantly attenuated with respect to the true target. We will refer to this second implementation as “missing-pulse implementation”.

A more significant extension of the range swath, with no appearance of any ghost, can be obtained if we accept to complicate the system by using two different carrier frequencies. This leads to the third implementation of the CopSAR concept, that we term “dual-frequency implementation”: the two sequences of pulses are both transmitted at rate $\mathrm{PRF}_1=\mathrm{PRF}_0/N_1$, but the first is transmitted at frequency f_1 and the second at frequency $f_2= (N_2/N_1)\, f_1$, so that wavelengths for the two sequences are related by $\lambda_2=(N_1/N_2)\, \lambda_1$. We are still assuming that N_1 and N_2 are two coprime integers and we still suggest to set $N_2 = N_1 +1$, if possible (see below). Therefore, replicas on the image $s_1(x,r)$ will be spaced according to

$$\Delta x_{i_1} = i_1\frac{\mathrm{PRF}_0\lambda_1 r_0}{N_1 2v} \quad , \quad \Delta r_{i_1} = \frac{\Delta x_{i_1}^2}{2r_0} \quad , \tag{14}$$

whereas replicas on $s_2(x,r)$ will be spaced according to

$$\Delta x_{i_2} = i_2 \frac{\mathrm{PRF}_0 \lambda_2 r_0}{N_1 2v} = i_2 \frac{\mathrm{PRF}_0 \lambda_1 r_0}{N_2 2v} \quad , \quad \Delta r_{i_2} = \frac{\Delta x_{i_2}^2}{2r_0} \quad , \tag{15}$$

so that, again, replicas on the two images will not be at the same location unless $i_1 = i\,N_1$ and $i_2 = i\,N_2$, that is

$$\Delta x_{i1} = \Delta x_{i2} = i \frac{\mathrm{PRF}_0 \lambda_1 r_0}{2v} = i \frac{N_2}{N_1} \frac{\mathrm{PRF}_0 \lambda_2 r_0}{2v} \quad , \tag{16}$$

and, also recalling that $N_1 < N_2$, all replicas in (16) will be suppressed by the AAP, so that no replica will appear in the final combined image obtained according to (7).

The pulses at the two frequencies can be transmitted at the same times if two different antennas are employed for the two frequencies, or the two sequences can be interlaced if a single antenna is used. In the former case the range swath size can be increased by a factor N_1, whereas in the latter it can be increased by a factor $N_1/2$. In both cases, the amount of data to be stored and processed is reduced by a factor $N_1/2$. It is worth noting that, although the dual-frequency design is certainly more complex, two- and even three-frequency space-borne SAR sensors have been already implemented in the past, see SIR-C/X-SAR [20] and SRTM [21] missions, and dual-frequency antenna design is well within reach of current technology, see, e.g., [22]. However, a practical limitation to the choice of the two carrier frequencies, and hence of N_1 and N_2, is given by the fact that the microwave frequency band is very "crowded", and very few frequency windows are available for SAR systems. Based on the bands assigned to SAR by current frequency allocation international regulations [23], possible choices are for instance to combine S band (for SAR: 3100 to 3300 MHz) with C band (5250 to 5570 MHz) to use N_1=3 and N_2=5, or the two allowed X-band windows (8550 to 8650 MHz and 9300 to 9900 MHz) to use N_1=7 and N_2=8, or also X band (9300 to 9900 MHz) with Ku band (13250 to 13750 MHz) to use N_1=5 and N_2=7.

At the end of this Section dedicated to practical CopSAR implementations, a few last words are needed about the effect of non-ideal AAP. In this case, CopSAR suffers from the same azimuth ambiguity problem as standard SAR, and techniques employed for the latter, e.g., [15], [19], can be easily adapted to deal with the former. In fact, we stress again that the aim of CopSAR is not to reduce azimuth ambiguity with respect to the standard SAR case, but rather to reduce the amount of data to be stored and processed, and, at the same time, to increase the range swath, without introducing significant additional ambiguities and without geometric resolution losses.

IV. Experimental Results

In this section we test the proposed approach by applying it to both simulated and real SAR raw signals. All the employed

simulated SAR raw signals have been generated by using the simulator of [24]-[25], and both simulated and real SAR raw signals have been processed to obtain focused SAR images by using the Fourier domain SAR processor provided in [2].

Let us first consider the basic CopSAR implementation, see Section III, and let us start with a simulated SAR raw signal obtained by employing the system parameters of the Sentinel-1 SAR sensor in HH polarization and stripmap acquisition mode, which are summarized in Table 1. In addition, we assume N_1=5 and N_2=6. First of all, in order to study the system impulse response function (IRF), we consider a scene in which only a point target with unitary amplitude is present. Azimuth cuts of the amplitudes of the aliased images $s_1(x,r)$ and $s_2(x,r)$ are shown in Figures 3 (a) and 3 (b). Replicas are clearly visible in these graphs: as theoretically expected, such replicas are progressively defocused, so that they are progressively attenuated and widened with respect to the central "true" target. In addition, the distance between replicas is 952 m for the first image and 793 m for the second, in agreement with the theoretical values of (4) and (5), and the smallest distance between replicas of the two images is 159 m, in agreement with (11). The amplitude of the azimuth cut of the final combined image $s(x,r)$, obtained by using (7), (i.e., the CopSAR IRF) is shown in Fig. 3 (c), whereas for reference purposes the amplitude of the azimuth cut of the standard SAR image (i.e, the standard SAR IRF) is plotted in Fig. 3 (d). It is clear that in the CopSAR IRF replicas are suppressed, and only a very small residual ambiguity due to sidelobes superposition is visible, as it can be better appreciated comparing the logarithmic plot of the CopSAR IRF in Fig. 4 (a) to the one of the standard SAR image in Fig. 4 (d). However, the level of this residual ambiguity amplitude is at about 1/100 of the level of the main lobe. In order to better verify the preservation of geometric resolution, in Fig. 5 we show an enlarged view of the region of the IRF around the main lobe. In this graph it is clear that the main lobe of the CopSAR and SAR IRFs have the same size, so that the geometric resolution is the same. However, the whole CopSAR IRF amplitude is decreased at $1/N_2$=1/6 of the SAR one, as theoretically expected, see Appendix A.

Let us now move to a more complex scene. The considered scenario is a very large ship (whose reflectivity function has been obtained from a real SAR image), oriented along the range direction, over a uniform, speckled dark background. The real ship is about 400 m long and 60 m wide, one of the largest container cargos in the world, and, for illustrative purposes, we here artificially even doubled its size. In this example, we again use the CopSAR approach with N_1=5 and N_2=6. Figures 6 (a) and 6 (b) show the amplitudes of the aliased multilook images $s_1(x,r)$ and $s_2(x,r)$ (spatial multilook over 4x4 pixel windows has been applied). Replicas of the target are evident. However, as it is clear from Fig. 6 (c), on the final combined image $s(x,r)$, obtained by using (7), replicas are suppressed, and only the true target appears. For comparison purposes, the image obtained in the standard SAR case (i.e., by processing the whole raw signal with no decimation) is shown in Fig. 6 (d). In order to better show that the CopSAR approach implies no resolution loss, in Fig. 7 we compare the full-resolution images obtained by using CopSAR, Fig. 7 (a), and standard SAR, Fig. 7 (d). It is evident that all ship details appearing in the standard SAR image are retained in the CopSAR one. The expected reduction of TBR, i.e., of the contrast with respect to the background, in the CopSAR

image is also evident. In fact, it turns out that the TBR in the CopSAR image is reduced by a factor 2.70 with respect to the one of the standard SAR image. This value should be compared to the theoretical (pessimistic) one of (25) in the Appendix, which in this case is equal to 3.27.

Let us now slightly modify the scene in order to consider the unfortunate case of a ship whose azimuth size does not satisfy condition (11). We consider the same SAR and CopSAR systems and the same scene of the previous example, but this time the ship is aligned along the azimuth direction. In addition, we have now used the true size of the ship, so that, from the viewpoint of target size, this is the most challenging situation that can be encountered in practice. The corresponding CopSAR and SAR images are shown in Figs. 8 (a) and 8 (b), respectively. Since the ship length (about 400 m) is larger than the value given by (11) (about 160 m), as expected ghosts appear on the image, in addition to the true target. However, if we compute the correlation coefficient between $s_1(x,r)$ and $s_2(x,r)$ over a window in correspondence of each bright spot of $s(x,r)$, it turns out that it is equal to 0.998 in correspondence of the central, true, target, and about 0.1 in correspondence of the ghosts. Accordingly, even in this very unfortunate situation, a correlation analysis allows us to distinguish the true target from ghosts, as theoretically predicted in Section II.

Let us now move to consider real data. The CopSAR approach has been applied to a real ERS-2 SAR raw signal, acquired on 10/10/2009 and freely available online [26], relative to a marine scene near the Long Beach harbor, Los Angeles, USA. The scene contains several ships, and it is close to the coast, so that it is particularly challenging for our approach. In addition, the sea background is not uniform. The raw signal has been properly decimated to obtain the two undersampled sub-sequences (again, N_1=5 and N_2=6) and then the two obtained decimated raw signals have been separately processed via the standard focusing algorithm of [2]. Figures 9 (a) and 9 (b) show the amplitudes of the aliased images $s_1(x,r)$ and $s_2(x,r)$, whereas Fig. 9 (c) shows the final combined image $s(x,r)$. For comparison purposes, the image obtained in the standard SAR case is shown in Fig. 9 (d). Spatial multilook over 4x1 (azimuth x range) pixel windows has been applied to obtain an approximately square pixel. Considerations similar to those made for the simulated case still hold also for these real data. Again, no resolution loss is obtained with respect to the standard SAR case, as it is clear by comparing Fig. 9 (c) and 9 (d). However, the expected reduction of TBR, and hence of the contrast with respect to the background, can be noticed. Note that in this case the sea background is not homogeneous: it is brighter in the left part, and in that area of the sea some features can also be noticed in the standard SAR image, see Fig. 9 (d), while such features are not visible in the CopSAR image of Fig. 9 (c), where that area of the sea appears substantially homogeneous. This confirms our theoretical expectation discussed in Section II.

Let us now move to the missing-pulse CopSAR implementation. The same simulated and real SAR raw signals of the previous case are considered, with N_1=5 and N_2=6, but, in the first sub-sequence, pulses that would be separated by just $1/PRF_0$ from a pulse of the other sequence are removed. Of course, in this case real ERS data have been used only for illustration purposes,

because the range swath actually cannot be increased. For the Sentinel-1 simulated data, the IRF of the CopSAR is shown in Fig. 10 (a): it is clear that in this implementation replicas are not completely suppressed, however, as theoretically predicted, the amplitude of such replicas is below $1/N_2=1/6$ of the true target one, as it can be better appreciated from the logarithmic plot of Fig. 4 (b). The enlarged view of the comparison of CopSAR and SAR IRFs of Fig. 10 (b) shows that also for this missing-pulse implementation geometrical resolution is preserved. With regard to the large ship scene, the amplitude of the aliased image $s_1(x,r)$ is shown in Figs. 11 (a) (the image $s_2(x,r)$ is the same as in the first implementation case), whereas the final combined image $s(x,r)$ is shown in Fig. 11 (b). This time, as expected from the discussion in the previous section, a larger number of replicas appear on the first image, Fig.11 (a), although not all with the same amplitude, and replicas appear also in the final combined image, Fig.11 (b), although they are significantly attenuated (by a factor of about 6, in the worst case) with respect to the true target. Reduction of the TBR with respect to the standard SAR case is here by a factor 3.51. Also in this case, however, no resolution loss is obtained with respect to the standard SAR case, as it is evident by comparing Fig. 7 (b) and 7 (d). Similar considerations can be done for the real ERS-2 SAR data, shown in Figs. 12 (a) and 12 (b) for $s_1(x,r)$ and $s(x,r)$, respectively (the image $s_2(x,r)$ is the same as in the first implementation case). Comparison with the standard SAR case can be made by comparing Figs. 12 (b) and 9 (d). This example shows that this missing-pulse implementation is particularly critical when several ships with very different returns are present in the same scene: in fact, replicas of very bright ships have intensities comparable to those of the true less bright ships.

Finally, let us consider the dual-frequency CopSAR implementation. This time we can use only simulated data, because real sensors operating at two "coprime" frequencies do not currently exist. The simulated scenario is the same as in the previous cases, and sensor's parameters are again those of Sentinel-1, except for the fact that a second, simultaneous acquisition at frequency equal to $N_2/N_1 = 6/5$ times the real sensor's frequency has been simulated, and that for both raw signals the PRF has been reduced by a factor $N_1=5$ with respect to the real sensor's one. The IRF of the CopSAR is shown in Fig. 13 (a): it is clear that in this implementation replicas are suppressed, and there is only a residual ambiguity due to sidelobe superposition, slightly higher than in the basic implementation (see also the logarithmic plot in Fig. 4 (c)). The enlarged view of the comparison of CopSAR and SAR IRFs of Fig. 13 (b) shows that also for this dual-frequency implementation geometrical resolution is preserved. With regard to the large ship scenario, in this dual-frequency case the image $s_1(x,r)$ is the same as in the basic implementation, Fig. 6 (a); the image $s_2(x,r)$ is reported in Fig. 14 (a), and the final combined image $s(x,r)$ is reported in Fig. 14 (b). The full-resolution image of the final combined image of the ship is reported in Fig.6 (c). It is evident that the images obtained in this case are very similar to those obtained in the basic implementation. Reduction of the TBR with respect to the standard SAR case is here by a factor 2.61. The advantage of this dual-frequency implementation is that the time separation between two consecutive pulses is increased by a factor $N_1=5$, so that the range swath can be extended by the same factor.

We have also performed simulations with parameter data of high-resolution space-borne X-band SAR sensors, namely COSMO/SkyMed and TerraSAR-X, and results are similar to those presented above. For these sensors, the maximum ship azimuth size, (11), is of the same order as that of Sentinel and ERS sensors, because the decrease of the wavelength λ is compensated for by the increase of the PRF_0 due to the higher azimuth resolution and, hence, the higher azimuth bandwidth. Another effect of using a higher carrier frequency is that replicas are less defocused than at lower frequencies [15], [19]. However, the CopSAR approach does not rely on replica defocusing to remove ambiguity due to sub-sampling, and therefore it is just affected by this phenomenon with regard to possible ambiguity due to non-ideal AAP, exactly as the standard SAR.

V. Conclusions

In this paper a new SAR technique has been presented that is able, in the case of bright targets over a dark background, to reduce the amount of data and, at the same time, to increase the range swath, with no resolution loss. The proposed approach is suitable to ocean monitoring for ship detection applications. The technique consists of a new SAR acquisition mode and of a very simple processing; it is based on the adaptation of the coprime array concept to the case of SAR systems, and therefore we have named it “Coprime SAR”, or, in short, “CopSAR”. Three different implementations have been proposed. The basic, simplest implementation can be even applied to currently available SAR sensor by properly decimating the sequence of received pulses, and it has been demonstrated by applying it to ERS-2 SAR raw data. However, this implementation only allows for a reduction of the amount of data to be stored and processed, but it does not allow an extension of the range swath. The second, “missing-pulse”, implementation allows further reducing the amount of data and doubling the range swath, but at the cost of the appearance of (significantly attenuated) ghosts on the image. Finally, a dual-frequency implementation allows both strongly reducing the data amount and significantly extending the range swath, with no appearance of ghosts. The approach effectiveness has been assessed by employing both simulated and real data. In particular, in the basic and dual-frequency implementations, the strong reduction of data amount and the significant increase of range swath (for the dual-frequency case) are only paid with a reduction of TBR and with the presence of a (non stringent) limit on ship azimuth size, but no resolution loss and no significant increase of ambiguities are obtained.

Note that in this paper we have applied the proposed CopSAR approach to stripmap SAR data, in order to use a very simple SAR processor to focus the images. This already allows, together with data reduction, a significant range swath improvement, especially in its dual-frequency implementation. However, the proposed approach can also be used in conjunction with the ScanSAR [17] or TOPSAR [25] acquisition modes, in order to further extend the range swath. Therefore, we believe that in future SAR systems it will be possible to combine CopSAR and ScanSAR modes to obtain very wide coverage images for maritime, ship detection applications. This goes beyond the scope of this paper, and it is left to future research.

APPENDIX A

In this Appendix, we theoretically analyze the TBR and the background statistics in the final CopSAR image obtained by using the rule of (7). Let us first consider a standard SAR complex image $s_0(x,r)$ of a scene constituted by a pointlike (or anyway small, satisfying (11)) deterministic target with amplitude T_0 over a uniform, darker background. We underline that the hypothesis of homogeneous background is here made to simplify the analysis, but it is not necessary for the practical application of the CopSAR approach. We also assume that that the background of $s_0(x,r)$ is a zero-mean circular complex random variable with standard deviation σ_0. This includes the case of fully developed speckle, in which we obtain a zero-mean circular Gaussian complex random variable, whose modulus is a Rayleigh random variable, and also the case of a partially developed speckle: in this latter case, a suitable model for a sea SAR complex image is the product of the squared root of a Gamma-distributed random variable and a zero-mean circular Gaussian complex random variable, so that the modulus of the resulting random variable is K-distributed [28]-[29]. According to the above assumptions, the TBR in the original SAR image is T_0^2/σ_0^2 .

If the raw signal is sub-sampled in azimuth by a factor N, then the number of in-phase contributions that form the focalized target is decreased by the same factor [2], so that the target amplitude is also reduced by a factor N, and its power is reduced by a factor N^2. Of course, the same holds for any point of the background, whose power will be then reduced by a factor N^2, too, so that it will be σ_0^2/N^2. However, since the background is a speckled distributed target, different aliased contributions will overlap on the same pixel of the aliased image: in particular, see Fig. 15, each pixel of the background will be the superposition of the baseband ("true") contribution and $2(N-1)$ statistically independent (because they come from far apart points) replicas, which will sum up incoherently, so that the pixel total power will be the sum of the powers of individual contributions (actually, if the Doppler bandwidth is significantly smaller than PRF_0, then the number of replicas may be smaller). This first of all implies that, even if in the original image the speckle is only partially developed, in the image obtained from the subsampled raw signal it will tend to be fully developed (because the number of scatterers that contribute to a pixel is larger). In addition, if we further assume an ideal AAP, a flat background power spectral density, and that the Doppler bandwidth is equal to PRF_0, then, see again Fig. 15, we will have couples of replicas whose powers are reduced with respect to the power of the baseband contribution by the factors $(N-1)/N$, $(N-2)/N$, ... , $1/N$. Accordingly, the power of the background of the image obtained from the subsampled raw signal will be

$$\frac{\sigma_0^2}{N^2}\left(1+2\sum_{i=1}^{N-1}\frac{i}{N}\right)=\frac{\sigma_0^2}{N^2}\cdot N=\frac{\sigma_0^2}{N} \quad . \tag{17}$$

Therefore, in the image obtained from the subsampled raw signal, while the power of the target is reduced by a factor N^2, the power of the background is only reduced by a factor N, so that the TBR is reduced by a factor N. Note that this evaluation is a bit pessimistic, because it assumes that the maximum possible number of replicas contributes to the background power.

In conclusion, considering two images $s_1(x,r)$ and $s_2(x,r)$ obtained from raw signals subsampled by factors N_1 and N_2 (with $N_1 < N_2$), respectively, target powers will be

$$T_1^2 = \frac{T_0^2}{N_1^2} \quad , \quad T_2^2 = \frac{T_0^2}{N_2^2} \ , \tag{18}$$

while background powers will be

$$\sigma_1^2 = \frac{\sigma_0^2}{N_1} \quad , \quad \sigma_2^2 = \frac{\sigma_0^2}{N_2} \ , \tag{19}$$

and these backgrounds will be with good approximation fully developed speckles, so that their moduli will be Rayleigh-distributed.

Let us finally consider the CopSAR image $s(x,r)$, obtained from the combination of $s_1(x,r)$ and $s_2(x,r)$ via (7). The target power T^2 will be

$$T^2 = \min\left(\frac{T_0^2}{N_1^2}, \frac{T_0^2}{N_2^2}\right) = \frac{T_0^2}{N_2^2} \ . \tag{20}$$

With regard to the background, the cumulative distribution function (CDF) of its modulus can be computed as:

$$F_y = \Pr\{\min(|s_1(x,r)|, |s_2(x,r)|) < y\} = 1 - \Pr\{\min(|s_1(x,r)|, |s_2(x,r)|) \geq y\} = 1 - \Pr\{|s_1(x,r)| \geq y, |s_2(x,r)| \geq y\} \quad , \tag{21}$$

where Pr stands for probability. Now we note that the contributions that overlap on a given pixel of the image s_1 come from different points with respect to the contributions that overlap on the same pixel of the image s_2, with the exception of the baseband ("true") contribution, which is the same in the two images. Accordingly, the two images can be considered with reasonable approximation as independent, and the joint probability in the last term of (21) can be approximated by the product of the marginal probabilities. By recalling that the CDF of a Rayleigh random variable of mean square value (i.e., power) $\sigma_{1,2}^2$ is

$$F_y = \Pr\{|s_{1,2}(x,r)| < y\} = 1 - e^{-\frac{y^2}{\sigma_{1,2}^2}} \quad , \tag{22}$$

and using (19), we get

$$F_y = 1 - e^{-\frac{y^2}{\sigma_1^2}} \cdot e^{-\frac{y^2}{\sigma_2^2}} = 1 - e^{-y^2\left(\frac{1}{\sigma_1^2}+\frac{1}{\sigma_2^2}\right)} = 1 - e^{-\frac{y^2(N_1+N_2)}{\sigma_0^2}} \quad , \tag{23}$$

which is the CDF of a Rayleigh random variable of power

$$\sigma^2 = \frac{\sigma_0^2}{N_1+N_2} \quad . \tag{24}$$

Finally, by taking the ratio of (20) and (24) we obtain that the TBR of the CopSAR image is $T^2(N_1+N_2)/(\sigma_0^2 N_2^2)$. Accordingly, in the final CopSAR image the TBR is reduced by a factor

$$N_2^2/(N_1+N_2) \tag{25}$$

with respect to the standard SAR image. Of course, due to the assumptions made, the value given by (25) is an approximated one, but, as shown in the examples of Section IV, it is not far from actually measured ones.

REFERENCES

[1] J. C. Curlander and R. N. McDonough, *Synthetic Aperture Radar: Systems and Signal Processing*. New York: Wiley, 1991.

[2] G. Franceschetti and R. Lanari, *Synthetic Aperture Radar Processing*. New York: CRC Press, 1999.

[3] A. Moreira, P. Prats-iraola, M. Younis, G. Krieger, I. Hajnsek, and K. P. Papathanassiou, "A Tutorial on Synthetic Aperture Radar," *IEEE Geoscience and Remote Sensing Magazine*, vol. 1, no. 1, pp. 6–43, 2013.

[4] M. Younis, C. Fischer, and W. Wiesbeck, "Digital Beamforming in SAR Systems," *IEEE Trans. Geosci. Remote Sens*., vol. 41, no. 71, pp. 1735–1739, 2003.

[5] N. Gebert, G. Krieger, and A. Moreira, "Digital Beamforming on Receive: Techniques and Optimization Strategies for High-Resolution Wide-Swath SAR Imaging," *IEEE Trans. Aerosp. Electron. Syst*., vol. 45, no. 2, pp. 564–592, 2009.

[6] M. Villano, G. Krieger, and A. Moreira, "Staggered SAR: High-Resolution Wide-Swath Imaging by Continuous PRI Variation," *IEEE Trans. Geosci. Remote Sens.*, vol. 52, no. 7, pp. 4462–4479, 2014.

[7] Wen-Qin Wang, "Space–Time Coding MIMO-OFDM SAR for High-Resolution Imaging", *IEEE Transactions on Geoscience and Remote Sensing*, vol. 49, no. 8, pp.3094-3104, 2011.

[8] G. Krieger, "MIMO-SAR: Opportunities and Pitfalls," *IEEE Trans. Geosci. Remote Sens.*, vol. 52, no. 5, pp. 2628–2645, 2014.

[9] Z. Li, H. Wang, T. Su, and Z. Bao, "Generation of Wide-Swath and High-Resolution SAR Images from Multichannel Small Spaceborne SAR Systems," *IEEE Geosci. Remote Sens. Lett.*, vol. 2, no. 1, pp. 82–86, 2005.

[10] W. M. Brown, G. G. Houser, and R. G. Jenkins, "Synthetic aperture processing with limited storage and presumming," *IEEE Transactions on Aerospace and Electronic Systems*, vol.9, pp. 166-176, 1973.

[11] M. Villano, G. Krieger, and V. Del Zoppo, "On-Board Doppler Filtering for Data Volume Reduction in Spaceborne SAR Systems", *Proceedings of the 15th International Radar Symposium*, pp.1-6, Gdansk (Poland), 2014.

[12] M. Tello Alonso, P. López-Dekker, and J. J. Mallorquí, "A Novel Strategy for Radar Imaging Based on Compressive Sensing", *IEEE Transactions on Geoscience and Remote Sensing*, vol. 48, no. 12, pp.4285-4295, 2010.

[13] V. M. Patel, G. R. Easley, D. M. Healy, and R. Chellappa, "Compressed synthetic aperture radar," *IEEE J. Sel. Topics Signal Process.*, vol. 4, no. 2, pp. 244–254, 2010.

[14] J. Fang, Z. Xu, B. Zhang, W. Hong, Y. Wu, "Fast Compressed Sensing SAR Imaging based on Approximated Observation", *IEEE Journal of Selected Topics in Applied Earth Observations and Remote Sensing*, vol.7 no. 1, pp: 352-363, 2014.

[15] R. K. Raney and G. J. Princz, "Reconsideration of Azimuth Ambiguities in SAR," *IEEE Trans. Geosci. Remote Sens.*, vol. 25, no. 6, pp. 783–787, Nov. 1987.

[16] P. Iervolino, M. Cohen, R. Guida, and P. Whittaker, "Ship-detection in SAR imagery using Low Pulse Repetition Frequency Radar," in *Proceedings EuSAR 2014*, pp. 1–4, Berlin (Germany), 2014.

[17] P. P. Vaidyanathan and P. Pal, "Sparse Sensing With Co-Prime Samplers and Arrays," *IEEE Trans. Signal Process.*, vol. 59, no. 2, pp. 573–586, 2011.

[18] P. P. Vaidyanathan and P. Pal, "Theory of Sparse Coprime Sensing in Multiple Dimensions," *IEEE Trans. Signal Process.*, vol. 59, no. 8, pp. 3592–3608, Aug. 2011.

[19] G. Di Martino, A. Iodice, D. Riccio, G. Ruello, "Filtering of Azimuth Ambiguity in Stripmap Synthetic Aperture Radar Images", *IEEE Journal of Selected Topics in Applied Earth Observations and Remote Sensing*, vol.7, no.9, pp. 3967–3978, 2014.

[20] R. L. Jordan, B. L. Huneycutt, and M. Werner, 'The SIR-C/X-SAR synthetic aperture radar system', *Proceedings of the IEEE.*, vol.79, no. 6, pp. 827–838, 1995.

[21] B. Rabus, M. Eineder, A. Roth, R. Bamler, "The shuttle radar topography mission—a new class of digital elevation models acquired by spaceborne radar", *ISPRS Journal of Photogrammetry and Remote Sensing*, vol. 57, no. 4, pp. 241–262, 2003.

[22] S. Maci and G. Biffi Gentili, "Dual-Frequency Patch Antennas", *IEEE Antennas and Propagation Magazine*, vol. 39, no. 6, pp.13-20, 1997.

[23] *Manual of Regulations and Procedures for Federal Radio Frequency Management*, U.S. Department of Commerce, National Telecommunications and Information Administration, Washington (USA), 2013.

[24] G. Franceschetti, M. Migliaccio, D. Riccio, G. Schirinzi, "SARAS: a SAR raw signal simulator", *IEEE Transactions on Geoscience and Remote Sensing*, vol. 30, pp.110-123, 1992.

[25] G. Franceschetti, A. Iodice, D. Riccio, G. Ruello, R. Siviero, "SAR Raw Signal Simulation of Oil Slicks in Ocean Environments", *IEEE Transactions on Geoscience and Remote Sensing*, vol. 40, no. 9, pp.1935-1949, 2002.

[26] http://eo-virtual-archive4.esa.int/

[27] F. De Zan, A. Monti Guarnieri, "TOPSAR: Terrain Observation by Progressive Scans", *IEEE Transactions on Geoscience and Remote Sensing*, vol. 44, no. 9, pp.2352-2360, 2006.

[28] E. Jakeman and P.N. Pusey, "A Model for Non-Rayleigh Sea Echo", *IEEE Transactions on Antennas and Propagation*, vol.24, no.6, pp.1145-1150, 1976.

[29] G. Di Martino, A. Iodice, D. Riccio, G. Ruello, "A Physical Approach for SAR Speckle Simulation: First Results", *European Journal of Remote Sensing*, vol. 46, pp. 823-836, 2013.

Figure 1. CopSAR concept, N_1=4, N_2=5: locations along the SAR line of flight at which pulses are transmitted. Blue: first sequence; red: second sequence; white: pulse not transmitted.

Figure 2. CopSAR concept, N_1=4, N_2=5, "missing-pulse" implementation: locations along the SAR line of flight at which pulses are transmitted. Blue: first sequence; red: second sequence; white: pulse not transmitted.

TABLE I
SENTINEL-1 SIMULATION PARAMETERS

Satellite height	[km]	693
Satellite velocity	[km/s]	7
Look angle	[°]	30
Azimuth antenna size	[m]	12.3
Range antenna size	[m]	5.5
Carrier frequency	[GHz]	5.405
Pulse duration	[μs]	35
Chirp bandwidth	[MHz]	60
Sampling rate	[Mhz]	60
PRF_0	[Hz]	1500
Doppler centroid	[Hz]	0

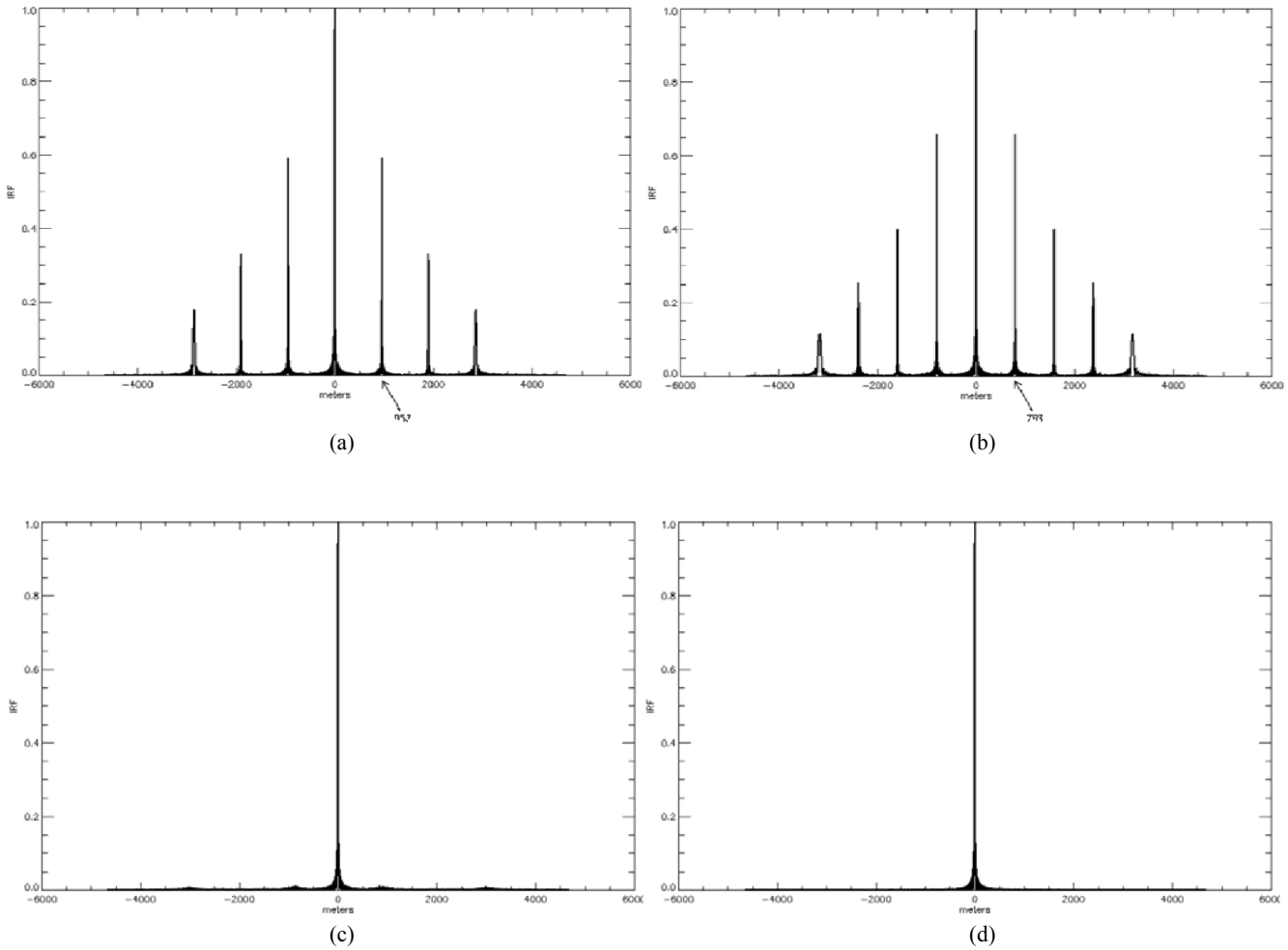

Figure 3. CopSAR basic implementation, N_1=5, N_2=6: amplitude azimuth IRFs of $s_1(x,r)$ (a), $s_2(x,r)$ (b), CopSAR (c), and standard SAR (d), normalized to their maximum value.

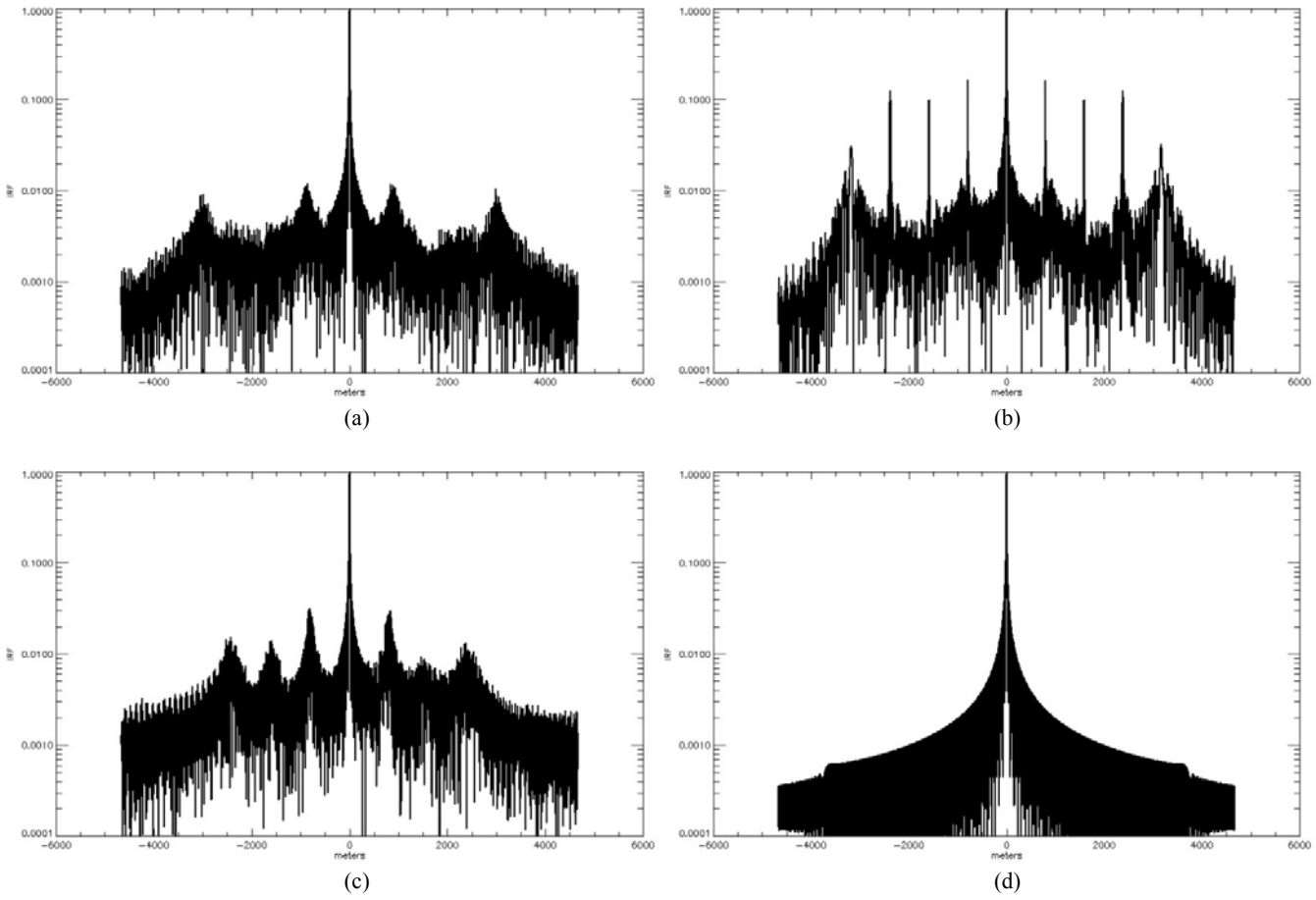

Figure 4. Logarithmic plots of amplitude azimuth IRFs normalized to their maximum value for the proposed CopSAR implementations (basic (a), missing pulse (b), and dual-frequency (c)) and the standard SAR image (d).

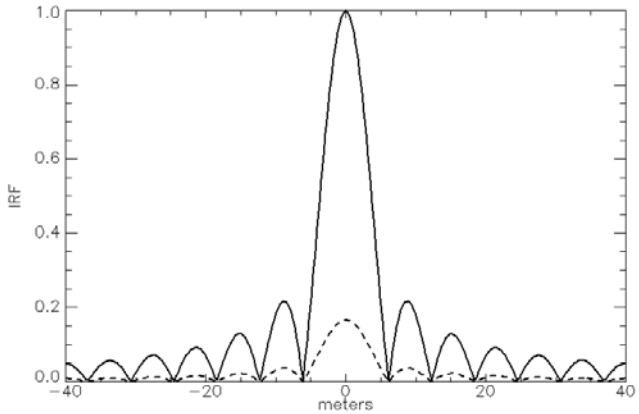

Figure 5. CopSAR basic implementation, N_1=5, N_2=6: enlarged view of amplitude azimuth IRFs of CopSAR (dashed line) and standard SAR (solid line), normalized to the maximum value of the standard SAR IRF.

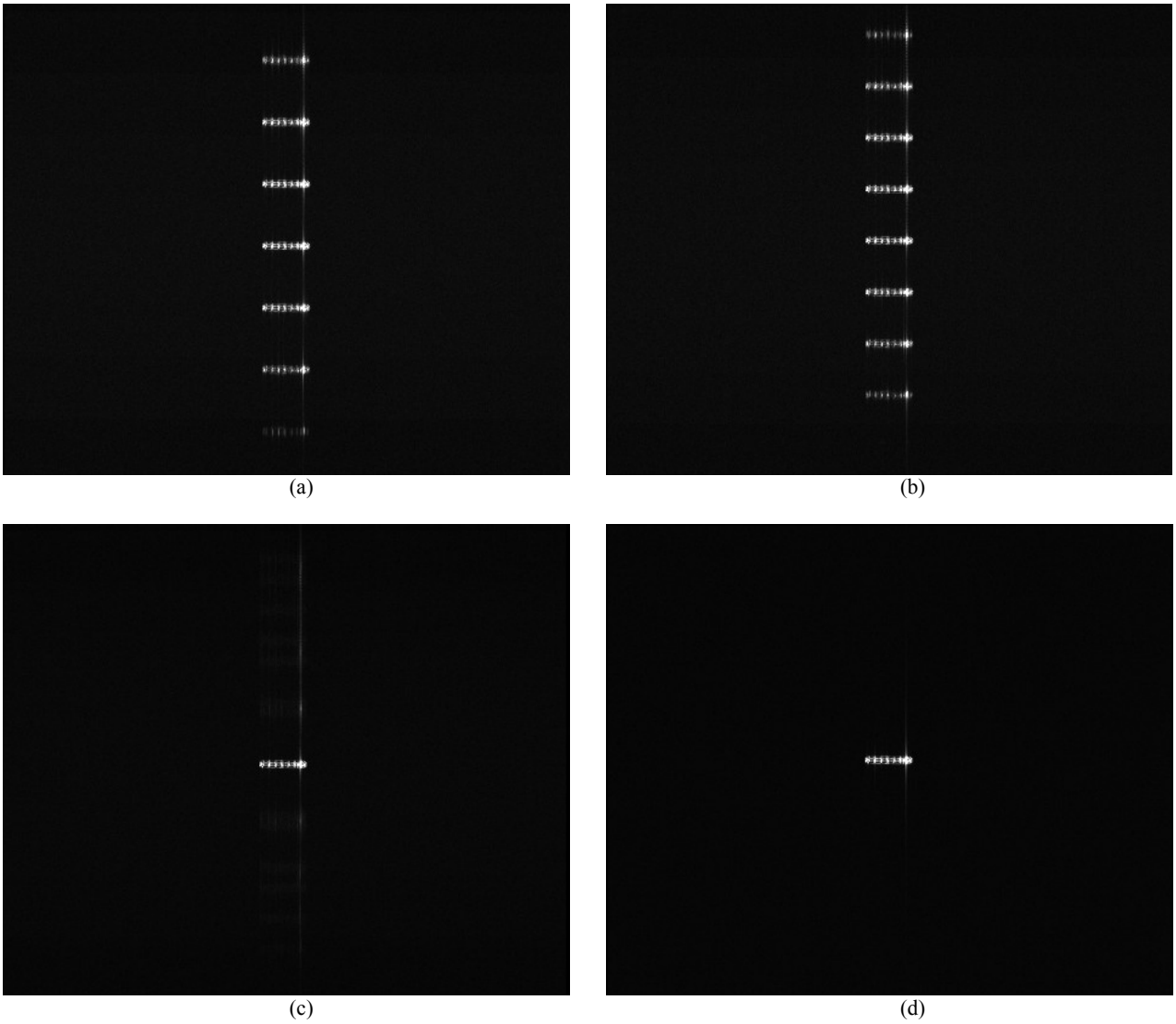

Figure 6. CopSAR basic implementation, N_1=5 and N_2=6: simulated images $s_1(x,r)$ (a) and $s_2(x,r)$ (b), the associated CopSAR image (c), and the standard SAR image processed with no decimation (d). A 4x4 multilook is applied.

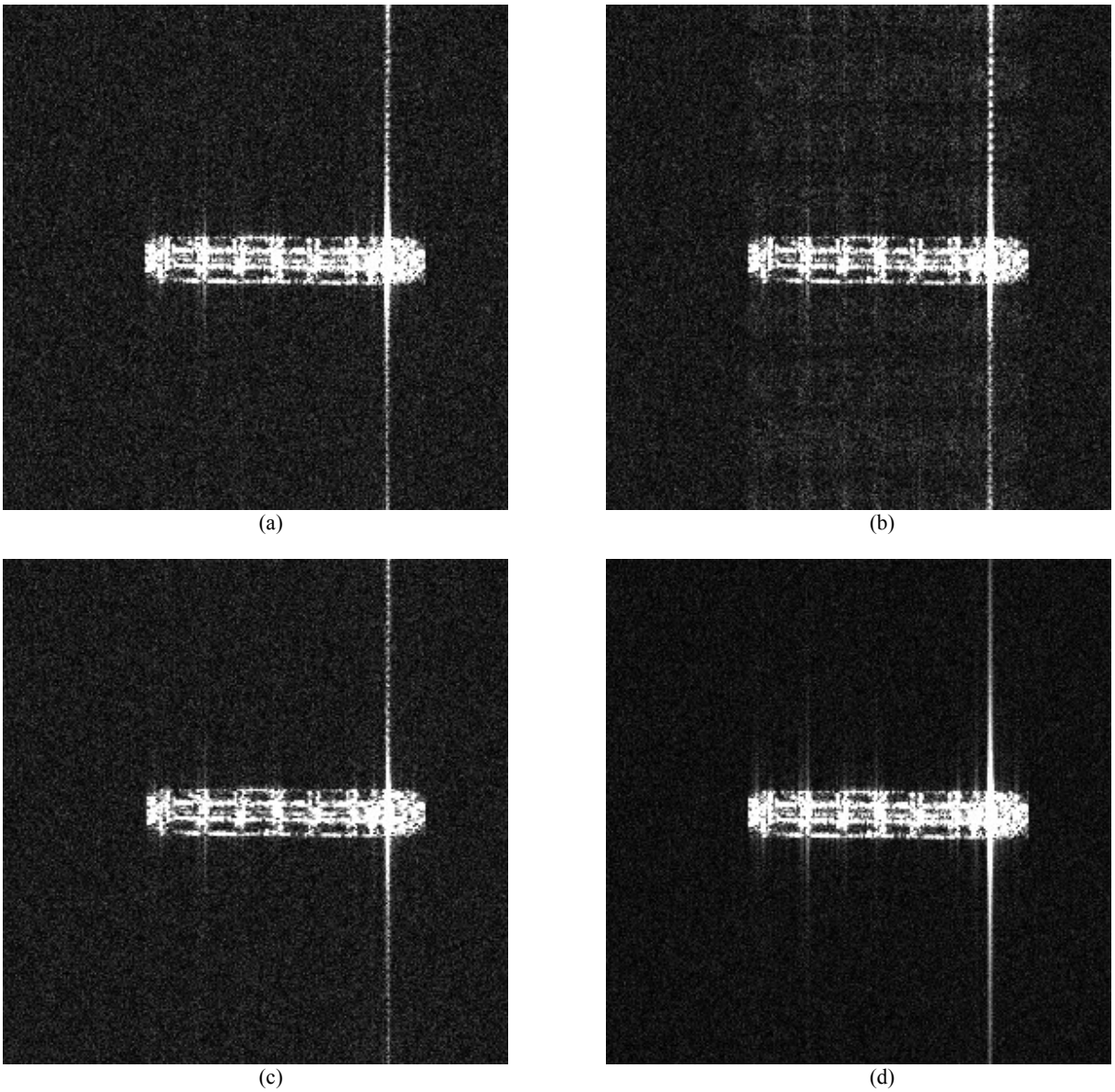

(a) (b)

(c) (d)

Figure 7. Full-resolution detail of the ship in Fig. 5: the three CopSAR implementations (basic (a), missing-pulse (b), and dual-frequency (c), respectively), and the standard SAR image (d).

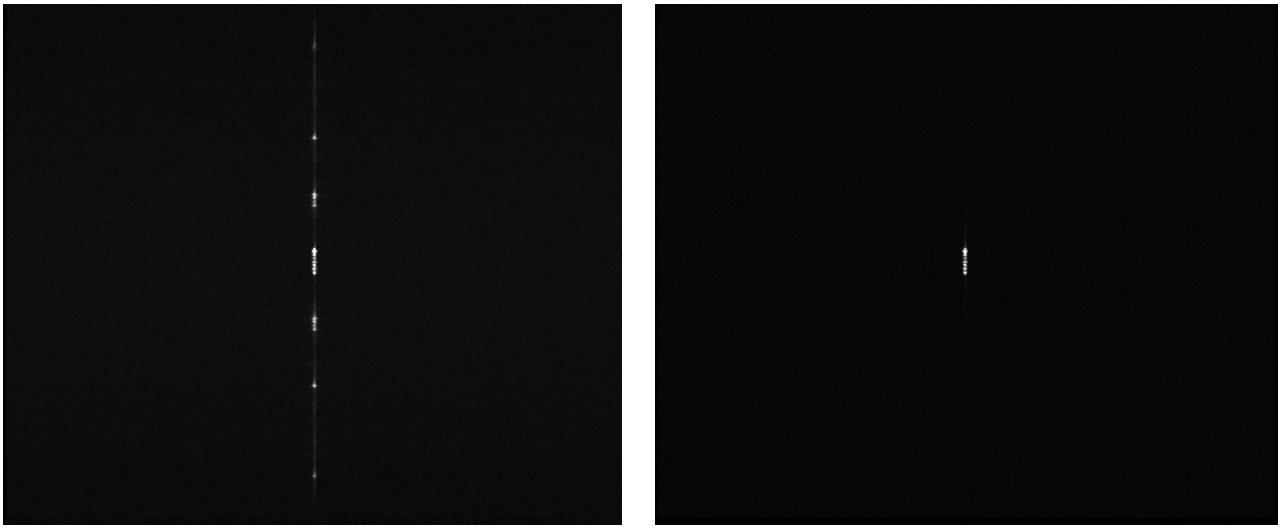

Figure 8. CopSAR basic implementation, N_1=5 and N_2=6: simulated CopSAR image (a), and the standard SAR image processed with no decimation (b). A 4x4 multilook is applied. The target does not satisfy condition (11).

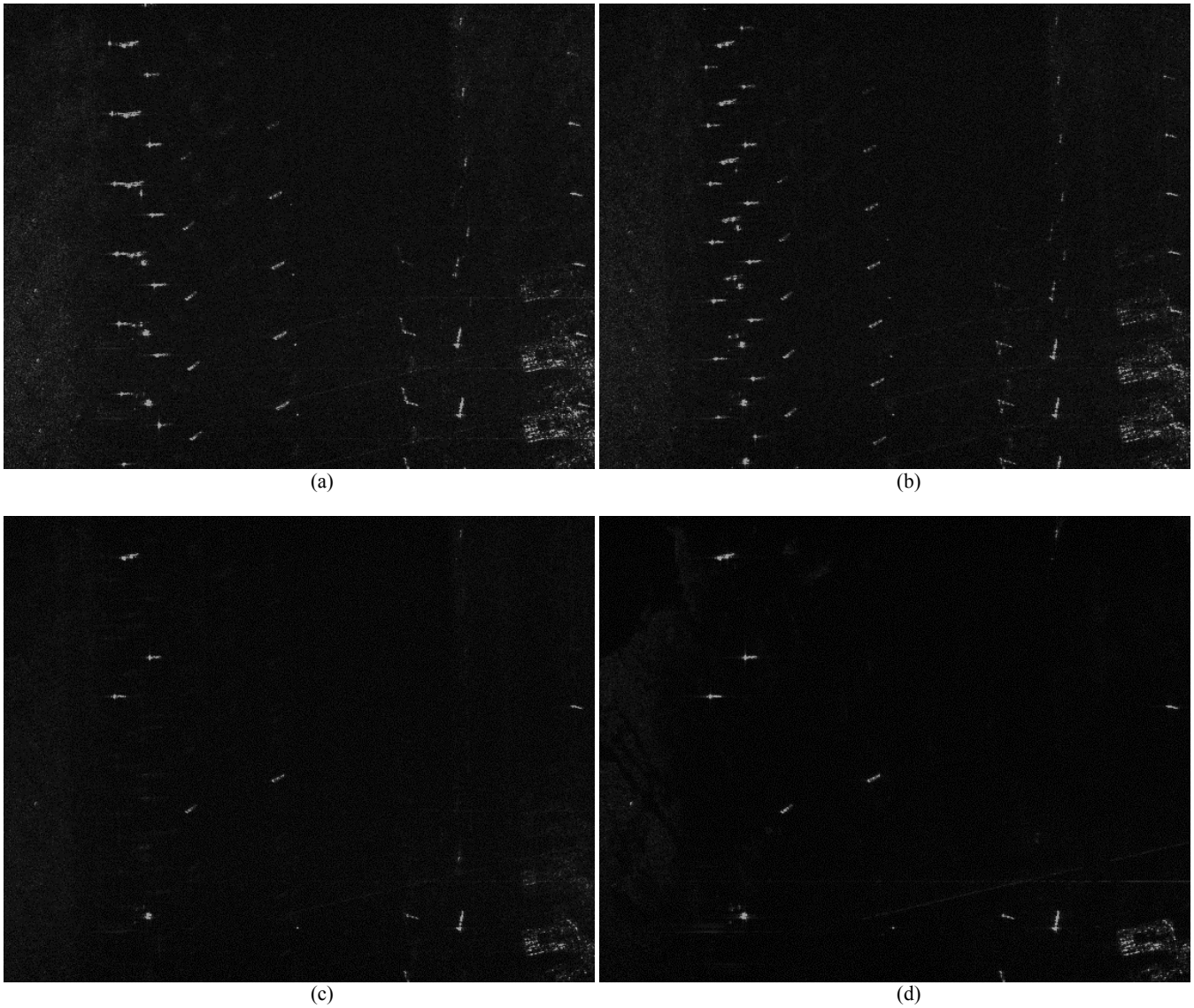

(a) (b)

(c) (d)

Figure 9. CopSAR basic implementation, N_1=5 and N_2=6: actual ERS images of an area close to the Long Beach harbor. Images $s_1(x,r)$ (a) and $s_2(x,r)$ (b), the associated CopSAR image (c), and the standard SAR image processed with no decimation (d). A 4x1 multilook is applied.

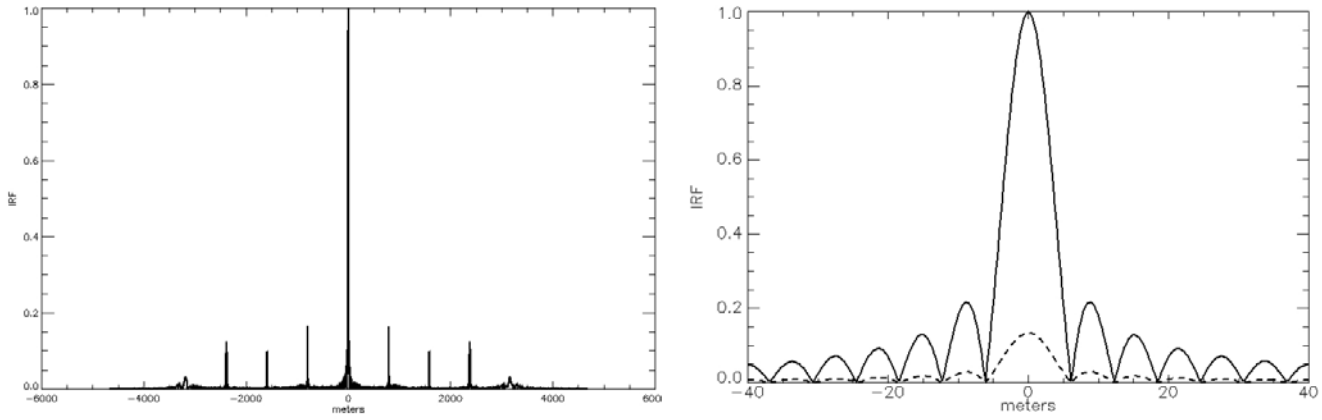

(a) (b)

Figure 10. CopSAR missing-pulse implementation, N_1=5, N_2=6: amplitude azimuth IRF of CopSAR normalized to its maximum value (a), and enlarged view of amplitude azimuth IRFs of CopSAR (dashed line) and standard SAR (solid line), normalized to the maximum value of the standard SAR IRF (b).

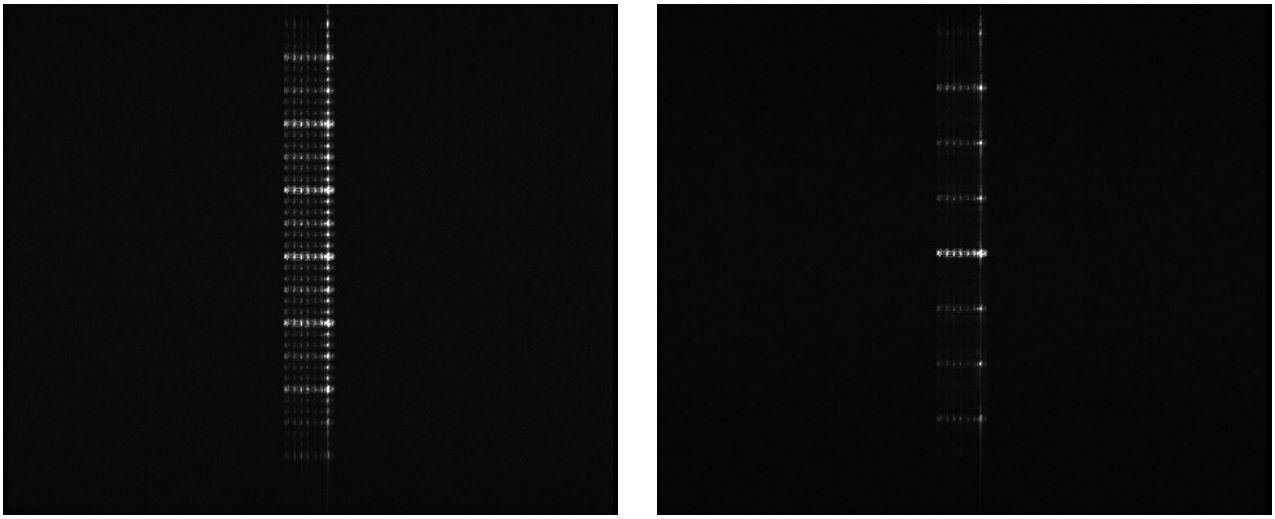

(a) (b)

Figure 11. CopSAR missing-pulse implementation, N_1=5 and N_2=6: simulated image $s_1(x,r)$ (a) and the associated CopSAR image (b). A 4x4 multilook is applied.

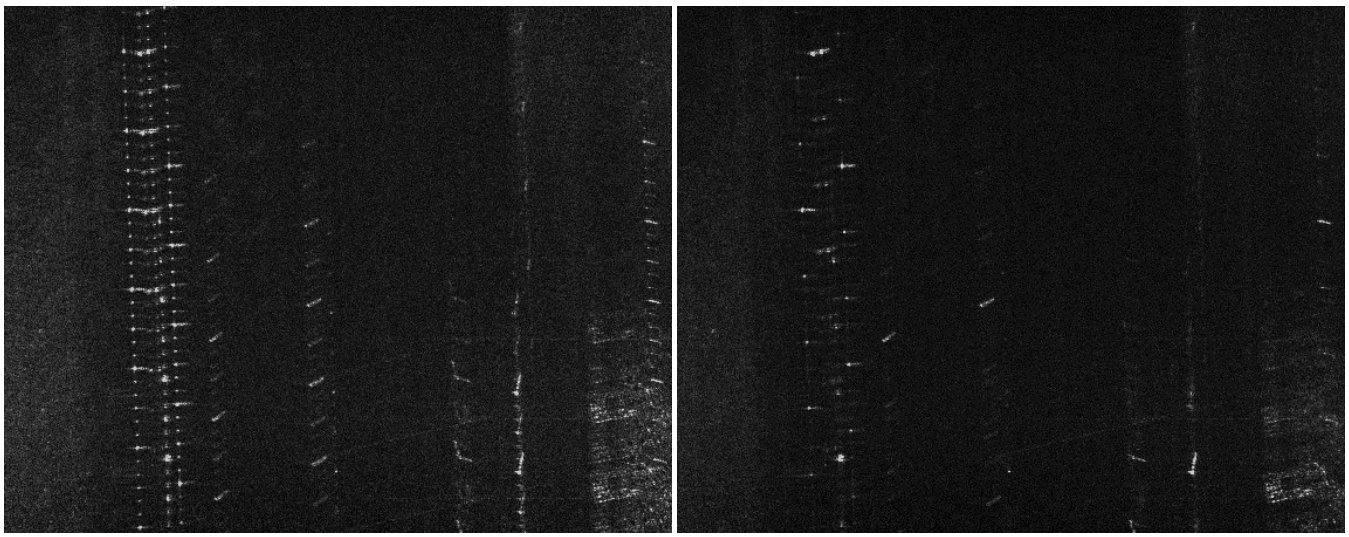

(a) (b)

Figure 12. CopSAR missing-pulse implementation, N_1=5 and N_2=6: actual ERS images of an area close to the Long Beach harbor. Image $s_1(x,r)$ (a) and the associated CopSAR image (b). A 4x1 multilook is applied.

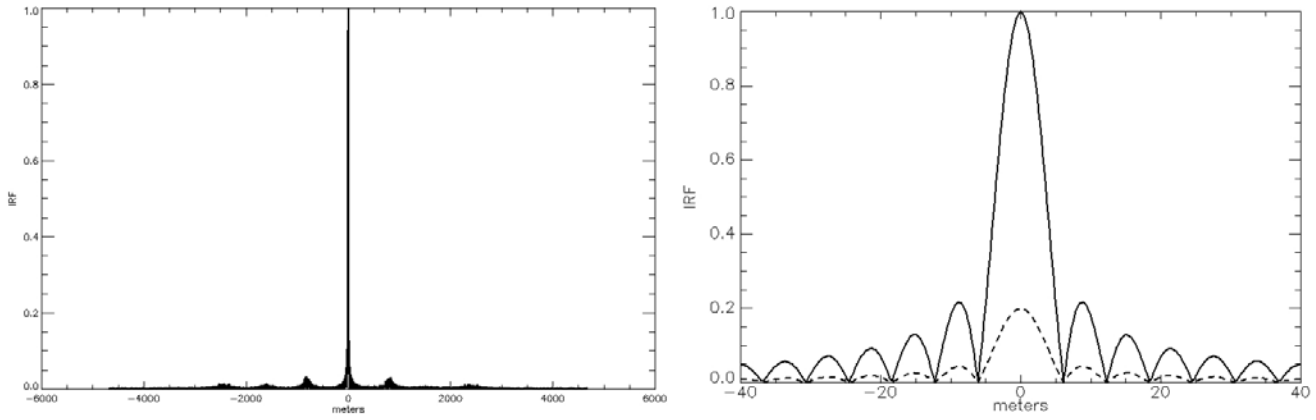

(a) (b)

Figure 13. CopSAR dual-frequency implementation, N_1=5, N_2=6: amplitude azimuth IRF of CopSAR normalized to its maximum value (a), and enlarged view of amplitude azimuth IRFs of CopSAR (dashed line) and standard SAR (solid line), normalized to the maximum value of the standard SAR IRF (b).

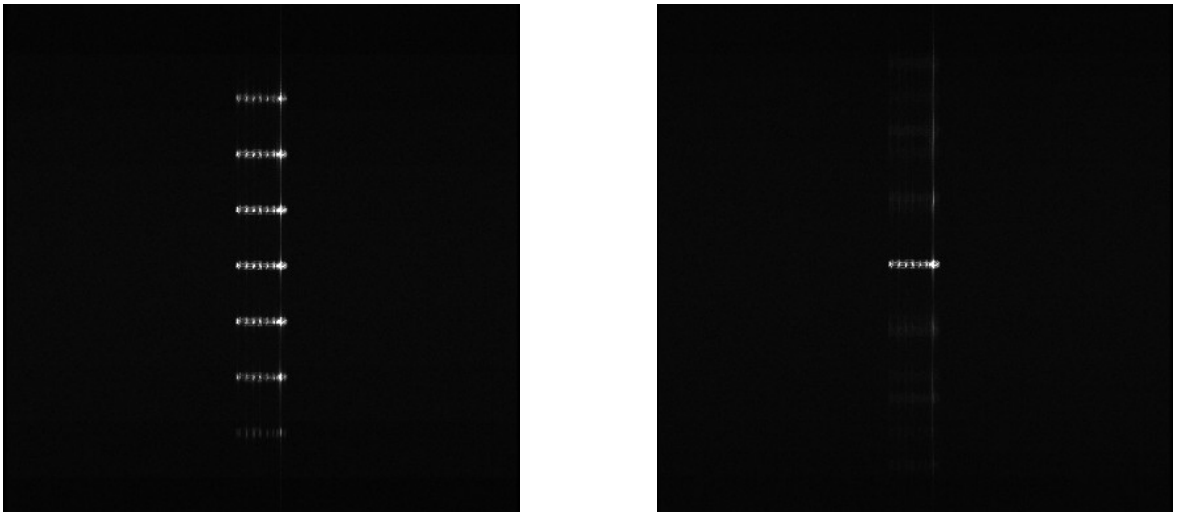

(a) (b)

Figure 14. CopSAR dual-frequency implementation, N_1=5 and N_2=6: simulated image $s_2(x,r)$ (a) and the associated CopSAR image (b). A 4x4 multilook is applied.

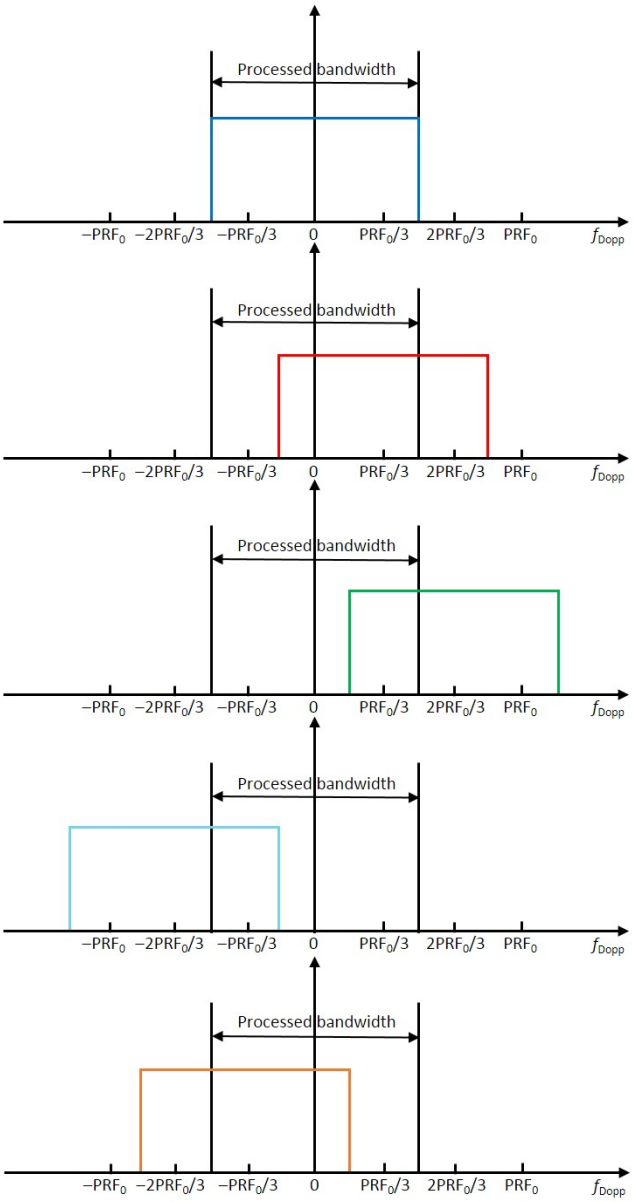

Figure 15. Spectral analysis of aliased overlapping contributions for the background, with a raw signal subsampling factor N=3. It is assumed that PRF_0 equals the Doppler bandwidth, so that the number of replicas is $2(N-1) = 4$. In-band power is maximum for the baseband contribution, and it decreases by the factors $(N-1)/N$, $(N-2)/N$, ... , $1/N$, i.e., 2/3 and 1/3, for the replicas.